SCIENCE CHINA
Information Sciences

• MOO PAPER •

May 2016, Vol. 59 053201:1–053201:7
doi: 10.1007/s11432-016-5553-5

A binocular vision-based UAVs autonomous aerial refueling platform

Haibin DUAN*, Han LI, Qinan LUO, Cong ZHANG, Cong LI, Pei LI & Yimin DENG

Bio-inspired Autonomous Flight Systems (BAFS) Research Group, School of Automation Science and Electrical Engineering, Beihang University (BUAA), Beijing 100191*, China*

Received January 28, 2016; accepted March 16, 2016; published online April 8, 2016

Abstract Unmanned aerial vehicles (UAVs) are highly focused and widely used in various domains, and the capability of autonomous aerial refueling (AAR) becomes increasingly important. Most of the research in this area concerns the verification of the algorithms while the experiments are conducted on the ground. In this work, in order to verify the vision system designed for boom approach AAR, an integrated platform is built and tested. The platform consists of a tanker UAV, a receiver UAV and a ground station. The pictures of the marker on the receiver UAV are captured by the binocular vision system on the tanker UAV and then used for flight control and boom control. Performance and feasibility of the platform are demonstrated by the real out-door flight tests, and the experimental results verified the feasibility and effectiveness of our developed binocular vision-based UAVs AAR.

Keywords unmanned aerial vehicles (UAVs), autonomous aerial refueling (AAR), boom approach, binocular vision, visual measurement

Citation Duan H B, Li H, Luo Q N, et al. A binocular vision-based UAVs autonomous aerial refueling platform. Sci China Inf Sci, 2016, 59(5): 053201, doi: 10.1007/s11432-016-5553-5

1 Introduction

Unmanned aerial vehicles (UAVs) are invaluable in today's military and civilian initiatives, especially in military operations, such as detecting moving targets [1,2], surveillance [3,4], and air combat [5]. However, most unmanned systems are being designed to execute the long-running mission. Thus, it is necessary for UAVs returning to the base for refueling [6]. Under this circumstance, autonomous aerial refueling (AAR) becomes an important capability for the future employment of UAVs. Vision based sensor and navigation system are widely used in AAR, while experiments are done for both probe-and-drogue refueling system [7–10] and boom approach [11,12]. To detect the drogue, a set of beacons mounted on the drogue can be supervised by a VisNav sensor [7], and 3D flash lidar is also used for drogue tracking [8]. For boom approach, a vision sensor based on visual snakes is developed in Ref. [11]. Furthermore, a sensor fusion between combined global position system (GPS)-based and machine vision-based measurements is proposed in Ref. [12].

* Corresponding author (email: hbduan@buaa.edu.cn)

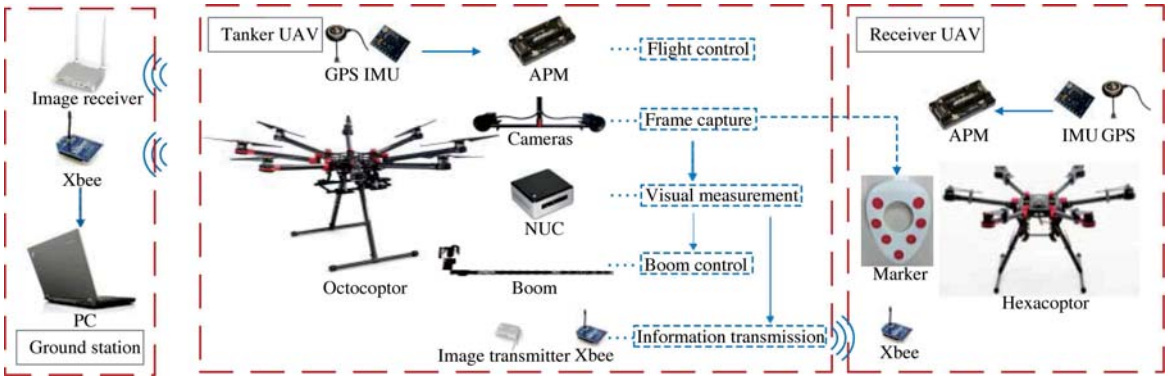

Figure 1 (Color online) Architecture of binocular vision-based UAVs autonomous aerial refueling platform.

However, the gap between algorithm simulation and practical application is quite big. In this work, a platform aiming to realize the real-time simulation of AAR in air is developed. The main components of the platform are two UAVs: an octocoptor serving as tanker UAV and a hexacoptor serving as receiver UAV. The GPS and inertial measurement unit (IMU) are used for remote navigation of the two UAVs. When the receiver arrives at the visual field of the cameras on the tanker (about 5 m), the binocular vision system will operate to capture the maker on the receiver. The on-board next unit computing (NUC) processes the images and estimates the pose of the receiver. Then the visual information obtained from the vision system is transferred to the flight controller and boom controller to control the flight of the UAVs and the movement of the boom towards receptacle. The communication between a ground station and UAVs, and in the inter-communication of the subcomponent of the UAV are realized through MAVlink protocol. In addition, the payload software is built in the framework of robot operating system (ROS), allowing us to add new functionality incrementally. Figure 1 shows the configuration of our binocular vision-based UAVs autonomous aerial refueling platform.

2 Binocular vision system for aerial refueling

This binocular vision system consists of two primary procedures: feature extraction and pose estimation. The pixel coordinates of red markers painted on the receiver UAV are generated after feature extraction. The generated pixel coordinates are utilized in the pose estimation process. Pose estimation procedure is exploited to calculate the relation matrix between the binocular vision system and marker coordination system [13].

2.1 Feature extraction

In this work, the space transformation from RGB to HSV is implemented to process each captured image. HSV space shows superior ability to describe color features of target compared with RGB space [14]. In order to segment the regions of image containing red markers, the upper and lower bound of hue and saturation channels of HSV image are selected to conduct the threshold segmentation. After HSV space transformation, the morphology methods including opening operation and closing operation are utilized to suppress image noise. Then, the class SimpleBlobDetector in OpenCV is exploited, which extracts contours of image after morphological processing and groups their centers to obtain blobs [15]. In the work, the upper and lower bound of area and circularity of blobs are set to filter noise blobs. Therefore, after extracting blobs, the area and circularity of each blob are calculated. Then, the blobs are output, which area and circularity are within the predefined range. The circularity of the blob C is defined as $C = 4\pi S/p^2$, and S is the area of the blob and p is the premise of the blob. The circularity of the standard circle is equal to 1. The centroid of each blob is calculated as the image coordinate of red marker, and the OpenCV function cvUndistortPoints is used for distortion correction of pixels of centers of extracted blobs.

2.2 Pose estimation

After the feature extraction process, points matching operation is conducted to obtain the index number of each feature point [16]. In this process, according to previous pose information, the world coordinates of markers are projected to the image plane. Specially, in the first frame, the image coordinates of the feature points are compared. According to the known geometrical relationship of the 7 points, the index number of the points can be obtained. The Euclidean distance matrix of projected points set $\{\hat{p}_1, \hat{p}_2, \ldots, \hat{p}_m\}$ and feature points set $\{p_1, p_2, \ldots, p_n\}$ is described as

$$Err = \begin{bmatrix} d(\hat{p}_1, p_1) & d(\hat{p}_1, p_2) & \cdots & d(\hat{p}_1, p_n) \\ d(\hat{p}_2, p_1) & d(\hat{p}_2, p_2) & \cdots & d(\hat{p}_2, p_n) \\ \vdots & \vdots & \vdots & \vdots \\ d(\hat{p}_m, p_1) & d(\hat{p}_m, p_2) & \cdots & d(\hat{p}_m, p_n) \end{bmatrix}. \tag{1}$$

In this work, Kuhn-Munkres algorithm [17] is applied to accomplish this point sets matching problem.

The binocular LHM algorithm based on the original LHM algorithm [18] is applied to accomplish pose estimation problem. The binocular LHM algorithm extends the original LHM algorithm by minimizing the object-space collinearity errors of two cameras. The left camera frame is defined as the unified coordinate frame of the binocular camera system. From the stereo camera calibration procedure, the translation and rotation matrix $[\, R^{rl} \;\; t^{rl} \,]_{3\times 4}$ from the right camera to the left camera are generated.

Given marker points $P_i (i = 1, \ldots, n)$ in the 3D reference, the image coordinates of ith marker measured by tth ($c \in \{l, r\}$) camera can be denotes as $p_i^c = [\, x_i^c \;\; y_i^c \;\; 1 \,]^{\mathrm{T}}$.

The relative position and attitude of the relative UAV are calculated by minimizing the quadratic sum of the linear errors in object space:

$$[R, t] = \arg\min \sum_{c=1}^{2} \sum_{i=1}^{n} \|e_i^c\|^2 = \arg\min \sum_{c=1}^{2} \sum_{i=1}^{n} \|(I - V_i^c)(RP_i + t - t^c)\|^2, \tag{2}$$

where $V_i^c = \frac{R^c p_i^c (R^c p_i^c)^{\mathrm{T}}}{(R^c p_i^c)^{\mathrm{T}} R^c p_i^c}$ and

$$[R^c \;\; t^c] = \begin{cases} [I \quad 0_{3\times 1}], & c = l, \\ [R^{rl} t^{rl}], & c = r. \end{cases}$$

The iteration method utilized in the original LHM is also exploited in the binocular LHM to obtain the final solution. In this work, the reprojection error is utilized to measure the accuracy of the algorithm. If reprojection error is smaller than 20, send the values of R and T to receiver UAV. When the reprojection error is larger than 20, the default matrix, a matrix saved the values of R and T of the last frame, is sent to the receiver UAV.

3 Boom system and formation controller

3.1 Boom system

To verify the effectiveness of our vision algorithm of the boom approach in AAR, we developed a mimical refueling boom system. After achieving the frame sequences of the marker on the receiver, the next unit computing (NUC) mounted onboard will conduct pose and position estimation. An arm microcontroller obtains the results, and figures out the control level to control steering engines [19]. Refueling boom will point at the receptacle in the resolved pose and position, and implement connect in air. The mechanical structure of our designed refueling boom is illustrated in Figure 2.

An installing base is used to fix power module and boom controller. The boom system is mounted under the base. Boom is a 2 m long two-stage rod. The boom diameter gradually changes from 6 mm to 12 mm, hollow on the inside. Motion mechanism consists of three servo motors. This structure well

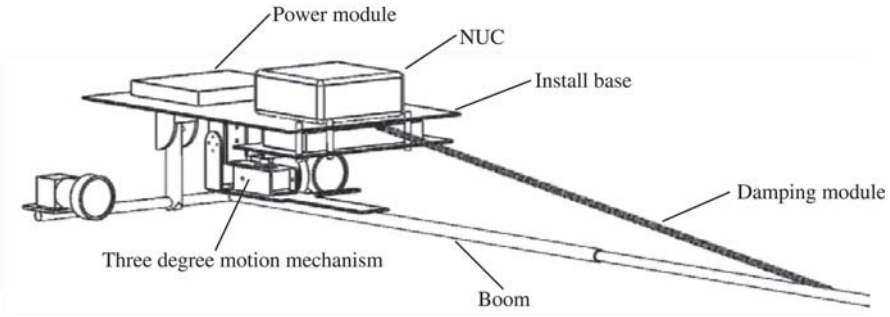

Figure 2 Mechanical structure of the boom.

realizes a three degree motion. Two helms controlling yaw and pitch have 90° motion displacement. While another helm can rotate two laps to stretch out and draw back the boom. An arm microcontroller receives visual results by serial communication, and computes the servo motors rotational angle, then sends instruction to the servo driving module. To reduce boom artifacts, two damping modules are fixed on the platform. A spring is embedded inside the boom to stretch out. Another spring connects up platform and boom, which can reduce artifacts greatly in yaw and pitch. The above-mentioned servo motors are perpendicular to each other. In this way, the moving region of boom can cover the probable connect position.

3.2 Modeling and control for a single UAV

Consider the earth-fixed frame E and the body frame B. Assuming that the center of mass of the quadrotor coincides with the body frame origin. The dynamic model of the quadrotor (Models for other multicoptors can be established in a similar way) can be written as follows [20,21]:

$$\begin{cases} \ddot{x} = (\cos\varphi\sin\theta\cos\psi + \sin\varphi\sin\psi)\,U_1/m, \\ \ddot{y} = (\cos\varphi\sin\theta\sin\psi - \sin\varphi\cos\psi)\,U_1/m, \\ \ddot{z} = -g + (\cos\varphi\cos\theta)\,U_1/m, \\ \ddot{\varphi} = \dot{\psi}\dot{\theta}(I_y - I_z)/I_x - \dot{\theta}\Omega J_R/I_x + U_2 l/I_x, \\ \ddot{\theta} = \dot{\psi}\dot{\varphi}(I_z - I_x)/I_y + \dot{\varphi}\Omega J_R/I_y + U_3 l/I_y, \\ \ddot{\psi} = \dot{\theta}\dot{\varphi}(I_x - I_y)/I_z + U_4 l/I_z, \end{cases} \tag{3}$$

where x, y, z are the translational motions in body frame, and φ, θ, ψ represent angular rotations along the body frame, which are roll angle, pitch angle and yaw angle, respectively. Besides, $I_{x,y,z}$ is the body inertia, J_R is the rotor inertia and l is length of the lever. Besides, $U_1 = b\left(\Omega_1^2 + \Omega_2^2 + \Omega_3^2 + \Omega_4^2\right)$, $U_2 = b\left(\Omega_4^2 - \Omega_2^2\right)$, $U_3 = b\left(\Omega_3^2 - \Omega_1^2\right)$, $U_3 = b\left(\Omega_2^2 + \Omega_4^2 - \Omega_1^2 - \Omega_3^2\right)$, $\Omega = b\left(\Omega_2 + \Omega_4 - \Omega_1 - \Omega_3\right)$, where b is the thrust factor and $\Omega_{1,2,3,4}$ are rotor speeds.

The system can be decoupled into two subsystems: the angular rotations and the linear translation. The widely used proportional-integral-derivative (PID) control technique was adopted in controller design since it is simple and straightforward to understand, which takes the form $\ddot{s} = k_P(s - s_d) + k_I \int (s - s_d)\mathrm{d}t + k_D(\dot{s} - \dot{s}_d)$, where s represents the state variable to be controlled.

3.3 Formation control based on potential field approach and binocular vision system

The refueling position is behind the tail of the tanker during the boom type refueling operation. The receiver is supposed to move and stay at the contact position, as shown in Figure 3. Simply, the three-dimensional motions of the receiver in airspace are decoupled into horizontal movement and vertical movement. Then the artificial potential field is designed in these two directions to guarantee that the receiver can move to the contact position very quickly and smoothly.

Goal position of the receiver relative to the tanker can be achieved and maintained by the artificial potential filed method, originally proposed by Khatib [22]. The potential field takes the following form

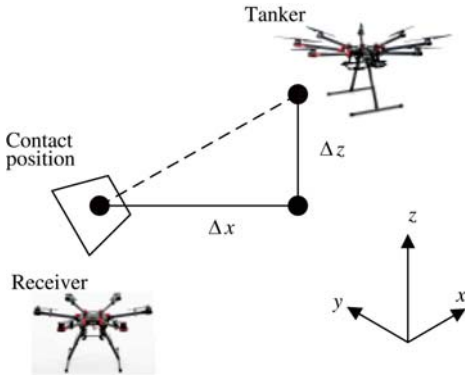

Figure 3 (Color online) Contact position for formation controller.

$U_{\text{total}}(q) = U_{\text{att}}(q) + U_{\text{rep}}(q)$. The command vector for the receiver that applies the designed potential field can be expressed as $F_{\text{total}} = F_{\text{att}} + F_{\text{rep}}$, where F_{att} represents an attractive force allowing the receiver to reach the desired position and F_{rep} represents a force inducing an artificial repulsion from the obstacle. The forces are gradients of the potential, that is $F_{\text{att}} = -\text{grad}(U_{\text{att}}(q))$, $F_{\text{rep}} = -\text{grad}(U_{\text{rep}}(q))$.

The attractive field can be defined as

$$U_{\text{att}}(q) = \frac{C_a}{1 + \exp(\rho^2(q, q_{\text{goal}}))}, \tag{4}$$

where C_a is a position gain and $\rho(q, q_{\text{goal}}) = \|q_{\text{goal}} - q\|$ represents the relative distance between the receiver and the contact position. This position is determined by the position of the tanker. The corresponding attractive force along the x, y, z axis can be obtained by taking partial derivatives of the attractive field, $F_{\text{att}}(x) = -\partial U_{\text{att}}/\partial x$, $F_{\text{att}}(y) = -\partial U_{\text{att}}/\partial y$, $F_{\text{att}}(y) = -\partial U_{\text{att}}/\partial z$.

The repulsive field can be expressed as

$$U_{\text{rep}}(q) = \begin{cases} \dfrac{1}{2} C_r \left(\dfrac{1}{\rho(q, q_{\text{obs}})} - \dfrac{1}{\rho_0} \right)^2, & \text{if } \rho(q, q_{\text{obs}}) \leqslant \rho_0, \\ 0, & \text{if } \rho(q, q_{\text{obs}}) > \rho_0, \end{cases} \tag{5}$$

where C_r is a position gain, $\rho(q, q_{\text{obs}}) = \|q_{\text{obs}} - q\|$ is the distance between receiver q and the obstacle q_{obs}. This repulsive force works only if the obstacle is within the predefined distance ρ_0. The repulsive forces can be expressed as

$$F_{\text{rep}}(x) = -\partial U_{\text{rep}}/\partial x, \quad F_{\text{rep}}(y) = -\partial U_{\text{rep}}/\partial y, \quad F_{\text{rep}}(y) = -\partial U_{\text{rep}}/\partial z. \tag{6}$$

4 Flight tests and result analysis

In order to verify the feasibility and effectiveness of this developed platform, a series of out-door flight tests are conducted in various environments, including strong and poor light conditions. Considering the safety and easy observation, the flight height of the UAVs is about 10 m. Since the tanker octocoptor blows a strong wind, the receiver hexacoptor can hardly fly too close to the tanker. However, it can be seen that the boom always moves to point at the receptacle following the relative movement between the UAVs.

Figure 4 shows the experimental results of binocular LHM algorithm. The red markers of receiver UAV are projected to the image frame based on the measured pose information.

The images captured with the on-board camera in low-light environment show the process of the docking phase (See Figure 5), and the out-door experimental results verified the effectiveness of our proposed approaches and designed binocular vision-based AAR platform.

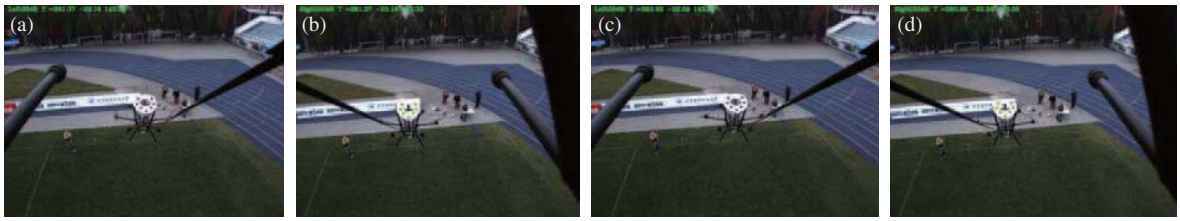

Figure 4 (Color online) The left frames captured on-board and the reprojection result on the corresponding right frame. (a) and (c) the feature extraction results on images captured with left camera; (b) and (d) relative projection result on images captured with right camera.

Figure 5 (Color online) The frames captured on-board show the process of the docking phase. (a) The receiver reaches the visual field of the binocular vision system and the pose estimation algorithm begins to work; (b) the receiver gets closer to the tanker; (c) the boom follows the motion of the receiver; (d) the boom points at the makers on the receiver, which indicates the system works well.

5 Conclusion

A binocular vision-based UAVs boom approach AAR platform is designed and implemented. In this platform, a binocular vision system is developed, while the flight controller and boom controller are also given. A series of out-door flight tests in various environments are conducted, and the experimental results verified the feasibility and effectiveness of our designed UAVs boom approach AAR platform. In the future, we will focus on the improvement of the stability and accuracy of binocular vision measurements in more complicated environments.

Acknowledgements This work was partially supported by National Natural Science Foundation of China (Grant Nos. 61425008, 61333004, 61273054) and Aeronautical Foundation of China (Grant No. 2015ZA51013).

Conflict of interest The authors declare that they have no conflict of interest.

Supporting information The supporting information is available online at info.scichina.com and link.springer.com. The supporting materials are published as submitted, without typesetting or editing. The responsibility for scientific accuracy and content remains entirely with the authors.

References

1 Tanner H G. Switched UAV-UGV cooperation scheme for target detection. In: Proceedings of IEEE International Conference on Robotics and Automation, Roma, 2007. 3457–3462
2 Wang X H, Duan H B. Biologically adaptive robust mean shift algorithm with cauchy predator-prey BBO and space variant resolution for unmanned helicopter formation. Sci China Inf Sci, 2014, 57: 112202
3 Jakob M, Semsch E, Pavlíček D, et al. Occlusion-aware multi-UAV surveillance of multiple urban areas. In: Proceedigns of the 6th Workshop on Agents in Traffic and Transportation, Toronto, 2010. 59–66
4 Duan H B, Qiu H X, Fan Y M. Unmanned aerial vehicle close formation cooperative control based on predatory escaping pigeon-inspired optimization (in Chinese). Sci Sin Tech, 2015, 45: 559–572
5 Baba Y, Takano H, Miyamoto S, et al. Air combat guidance law for an UCAV. In: Proceedings of the 1st Technical Conference and Workshop on Unmanned Aerospace Vehicles, Portsmouth, 2002. 1–11
6 Nalepka J P, Hinchman J L. Automated aerial refueling: extending the effectiveness of unmanned air vehicles. In: Proceedings of Modeling and Simulation Technologies Conference and Exhibit, San Francisco, 2005. 15–18
7 Valasek J, Gunnam K, Kimmett J, et al. Vision-based sensor and navigation system for autonomous air refueling. J Guid Control Dyna, 2005, 28: 979–989

8 Chen C I, Stettner R. Drogue tracking using 3D flash lidar for autonomous aerial refueling. Proc SPIE Laser Radar Technology and Applications XVI, 2011, 80370Q
9 Yin Y, Xu D, Wang X, et al. Detection and tracking strategies for autonomous aerial refueling tasks based on monocular vision. Int J Advanced Robot Syst, 2014, 11: 1–12
10 Wilson D B, Goktogan A H, Sukkarieh S. Experimental validation of a drogue estimation algorithm for autonomous aerial refueling. In: Proceedings of IEEE International Conference on Robotics and Automation (ICRA), Seattle, 2015. 5318–5323
11 Campa G, Fravolini M L, Ficola A, et al. Autonomous aerial refueling for UAVs using a combined GPS-machine vision guidance. In: Proceedings of Guidance, Navigation, and Control Conference and Exhibit, Providence, 2004. 1–11
12 Doebbler J, Spaeth T, Valasek J, et al. Boom and receptacle autonomous air refueling using visual snake optical sensor. J Guid Control Dynam, 2007, 30: 1753–1769
13 Zhang S J, Cao X B, Zhang F, et al. Monocular vision-based iterative pose estimation algorithm from corresponding feature points. Sci China Inf Sci, 2010, 53: 1682–1696
14 Lei T, Wang Y, Fan Y Y, et al. Vector morphological operators in HSV color space. Sci China Inf Sci, 2013, 56: 1–12
15 Zhang W L, Liu L B, Yin S Y, et al. An efficient VLSI architecture of speeded-up robust feature extraction for high resolution and high frame rate video. Sci China Inf Sci, 2013, 56: 1–14
16 Duan H B, Zhang Q F, Deng Y M, et al. Biologically eagle-eye-based autonomous aerial refueling for unmanned aerial vehicles. Chinese J Sci Instrum, 2014, 35: 1450–1458
17 Kimmett J, Valasek J, Junkins J L. Autonomous aerial refueling utilizing a vision based navigation system. In: Proceedings of the Guidance, Navigation and Control Conference and Exhibit, Monterey, 2002. 1–11
18 Lu C P, Hager G D, Mjolsness E. Fast and globally convergent pose estimation from video images. IEEE Trans Pattern Anal Mach Intell, 2000, 22: 610–622
19 Chen S Z, Xu H, Liu D K, et al. A vision of IoT: applications, challenges and opportunities, with China perspective. IEEE Int Things J, 2014, 1: 349–359
20 Bouabdallah S, Siegwart R. Full control of a quadrotor. In: Proceedings of IEEE/RSJ International Conference on Intelligent Robots and Systems, San Diego, 2007. 153–158
21 Bouabdallah S, Murrieri P, Siegwart R. Design and control of an indoor micro quadrotor. In: Proceedings of IEEE International Conference on Robotics and Automation (ICRA'04), New Orleans, 2004, 5: 4393–4398
22 Khatib O. Real-time obstacle avoidance for manipulators and mobile robots. Int J Robot Res, 1986, 5: 90–98